Unsheathing the Vibrational Dynamics of Swords

Kenneth Marut and Tyler Michael

ABSTRACT

In this study, the vibrational characteristics of a select batch of different swords were resolved in order to locate and analyze vibrational nodes of the first two bending modes. These nodes were used to specify a "sweet spot" or region where the user would feel the least amount of vibration at the hilt when an object was miss hit. The three swords that were selected for testing were a German long sword, Spanish bullfighting sword, and a Japanese Katana sword. Autodesk Simulation Mechanical software was used to generate finite element models and calculate mode shapes and natural frequencies of the swords in a free-free boundary condition. Alongside the simulations, experiments were completed using a force hammer to provide an impulse while monitoring blade and hilt dynamics with a single point laser vibrometer. The experiments were used to validate the model and also to review each sword critically to provide an answer as to which sword is best in terms of reducing pain experience by the user at the hilt of the sword.

INTRODUCTION

Background

Throughout history, swords have been used by cultures all over the world for close range combat, dating all the way back to about 3300 BC. Across the world and over the course of thousands of years swords have evolved very differently due to available manufacturing methods, materials, and cultural differences. Regardless of the evolution, swords have managed to keep the same general morphology of a metal blade attached to a hilt. Outside of the broad characteristics, small variances remain, as many swords now exist of varying geometries, weights, and material composition. A diagram showing general sword terminology that will be used through this report is shown below in Figure 1.

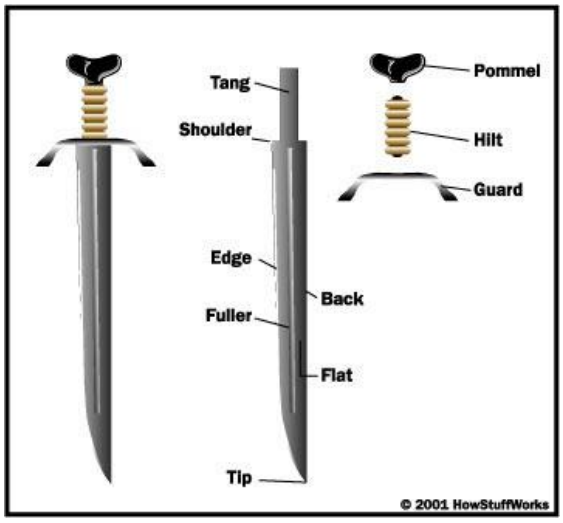

Figure 1. A sword schematic to show the composition of the blade, how the tang is inserted into the hilt, and how the handle is composed of three parts (http://science.howstuffworks.com/sword-making1.htm).

The goal of this research project is to investigate the vibrational properties of 3 different swords comparing our modeling techniques to experimental results. When struck by an impulse on the broad side of the blade, a sword will vibrate at its natural frequencies, yielding bending mode shapes as well and associated nodes along the hilt and blade at which vibrational displacement is zero. By observing the operational deflection shapes of each sword we want to determine which sword morphologies are the

most desirable with regards to mitigated vibration felt by the user upon a miss hit. Here in this study we will define a miss hit as contact that happens when the cutting edge is not exactly perpendicular to the normal plane of its target.

"Sweet Spot" Analysis

The "sweet spot" of a tool or weapon such as a sword, baseball bat, tennis racquet, etc. lacks a proper definition. In essence, the sweet spot refers to a point or zone of the hand-held object that when struck, produces minimal sensation in the gripping hand with minimal energy or shock transferred to the holder. Several definitions for the sweet spots include: the location where maximum energy is transferred to the point of impact, the center of percussion, the node of the fundamental vibrational mode, and so on [1]. For this study, we investigate the nodes that occur during the first and second modes of each sword to determine a sweet spot "range". This method of analysis was inspired by a physicist from the University of Sydney who did a similar analysis on baseball bats. Figure 2 shows the first two bending modes of the baseball bat that were derived from this study. For this study and that of Cross, the first two bending modes are the only observed modes because they are associated with the highest energy transfers [2]. The red markers indicate the nodes of the first mode and the black markers indicate the nodes of the second mode. For the bat we can identify two zones where the first and second nodes are relatively close to each other. One zone is on the handle which we will call the hilt node for our analysis. The second is on the large part of the bat which we will call the blade node [2].

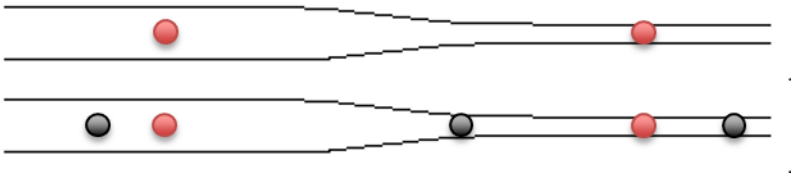

Figure 2. The first two bending modes with their nodes highlighted of a free-free baseball bat. The red dots correspond to the first mode and the black belong to the second.

The desire for the hilt nodes is that they be close enough together that the user can cover the zoned created with his or her hand(s). The distance apart of the blade nodes is more important as the zone of impact and would ideally converge upon zero in a perfect design. This would mean that in hitting the same sweet spot both the first and second modes would not be excited. If there nodes are close but not equal then one mode will not be excited will the other will excite at an energy level proportional to the distance from the other blade node.

METHODS AND MATERIALS

Sword Selection

Three swords were selected for testing: German long sword measuring 46.38 inches in length, Spanish bullfighting sword measuring 30.33 inches, and a Japanese Katana sword measuring 40.87 inches (Figure 3). The swords were selected due to their fundamentally different morphologies, geographic/cultural differences, and also due to their availability. It is important to note that the selected swords were all replica swords, thus their methods of manufacture are most likely untrue to the original swords that they are derived from.

Figure 3. Photographs taken of all three swords. From the top: long sword, Spanish sword, and Samurai sword.

CAD Modeling

CAD models of the 3 selected swords were generated using Autodesk Inventor CAD software. A digital picture of each sword was taken and digitized to create a 2-dimensional digital sketch. Using the 2-D sketch and digital calipers, the full 3-D geometries of each sword were generated. An assembly was created for each sword so that the different components (consisting of different materials) were taken into account. Figure 4 shows the completed CAD models of each sword. It is important to mention that the geometry of the tang of each sword, (the extension of the blade into the handle), was approximated as we were unable to disassemble the swords to measure the inner dimensions.

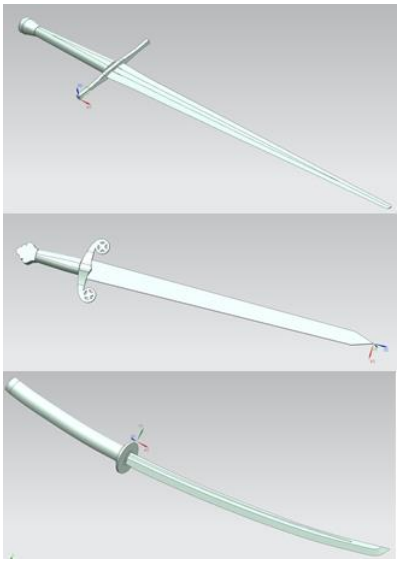

Figure 4. CAD images of the three models generated for each sword and input into the Autodesk simulator. From the top: long, Spanish, and samurai sword.

Finite Element Analysis

Using Autodesk Simulation Mechanical (ASM) software, finite element models of each sword were generated using the original CAD models. Meshing size was automatically determined using the

built in auto-meshing tool in the ASM software. Material properties were assigned to each separate component of the CAD sword assemblies from the built in material library. A caveat to this work is that some material properties of the swords were unable to be determined (i.e. the metal type of the blade and wood type of the hilt). Therefore we assumed a standard AISI 5150 type steel for the blade, and European Walnut wood for the hilt if the components were unknown. A modal analysis simulation was completed for each sword in order to determine the first 3 transverse bending mode shapes and frequencies. Data for the displacement along the sword was collected to determine node locations of the first 2 bending modes.

Experimental Setup

Each sword was measured for total length and 21 pieces of reflective tape where placed at 5% of intervals along the sword from pommel to tip. Each hammer/measuring point will be referred to as l_m where the m index runs from 0 to 20. Each measuring point was struck by a force hammer 4 times and averaged to create one data set per point. The laser vibrometer measurement was taken at two separate points, point A and B residing at 9 and 15 respectively, for each averaging process which yielded two data sets per point per sword. The laser vibrometer was placed directly above the swords on the same table mounted to a tripod. A SigLab system was used to extract the laser vibrometer velocities and create each data set. The mount used to hold each sword was made up of four 80/20 posts with 3 rubber bands tied around each post and clamped to a constant height for free-free boundary condition in the experiments. The free-free condition is justified because the clamping nature of a human hand does not affect the modes shapes or frequencies that much it just serves to dampen the vibration of the hand held object [2]. The full setup can be seen below in Figure 5.

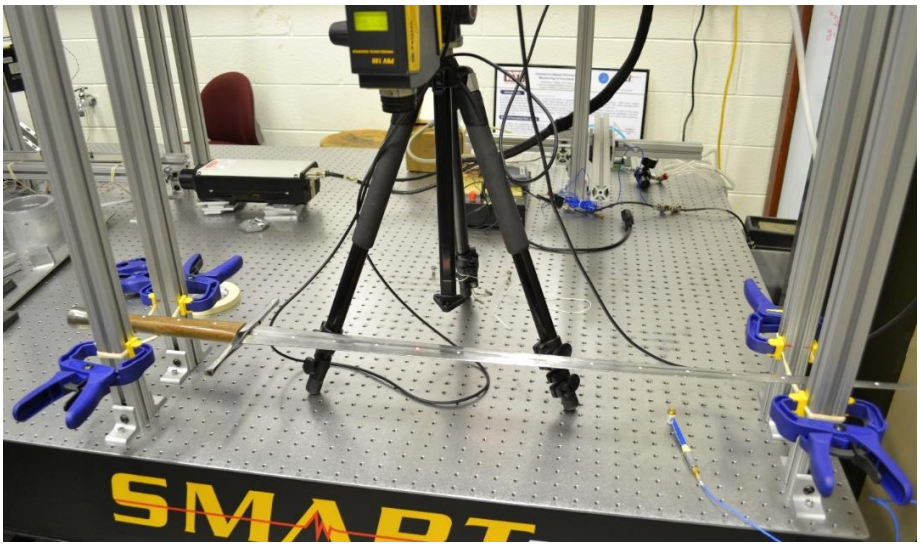

Figure 5. A picture of our experimental setup with the long sword placed on the mount. Rubber bands around posts were used to simulate a free-free condition. The laser vibrometer was placed directly above the blade and focused on one pre-determined point.

RESULTS

Experimental

For the experiments we never moved the laser in one trial and struck each measurement point with the force hammer to obtain velocity measurements for the specific point struck by the hammer. We rationalized this with the assumption that our system would be linear and Maxwell's reciprocity theorem would hold up. Meaning if the sword is struck at point a and measured at point b the output should be the same as if struck at point b and measured at point a. An example output of a single run, averaged three

times, of the long sword is shown in Figure 6. Coherence values for our measurement at each resonant frequency remained above 0.9 and varied by experiment in between that value and 1.0. The magnitude of the transfer function is shown on the top and the phase on the bottom of Figure 6.

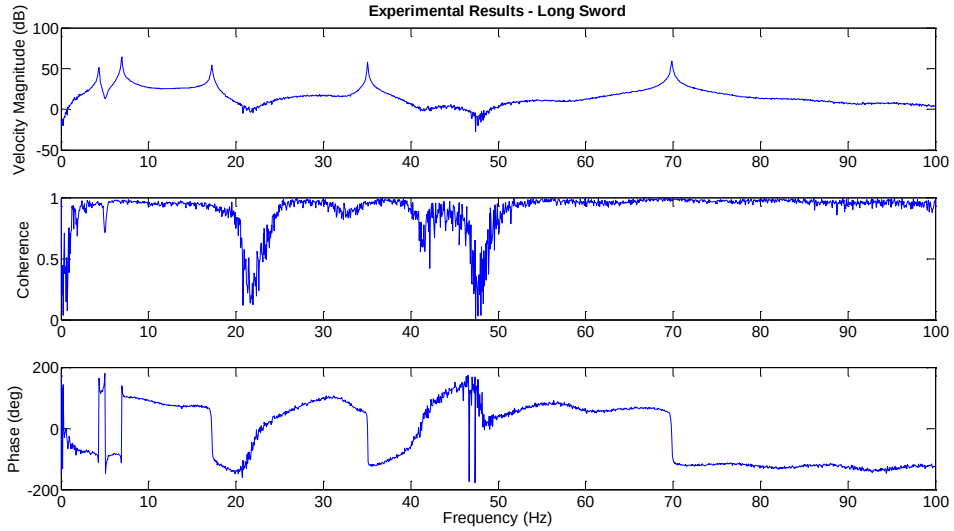

Figure 6. An example output from our SigLab system with the long sword on the testing stand measuring from point b and striking from point a. From the top: magnitude of transfer function ignoring complex format, coherence, and phase as a function of frequency.

Each experimental run for both points A and B were used to find the resonant frequencies of each sword. A MATLAB peak finding algorithm was used to find the frequency value of each peak in the magnitude of the transfer function. These values were averaged to find the first three bending mode frequencies. Figure 7 shows the experimentally resolved frequencies and Table 1 has the numerical values of these modes for reference. The samurai sword was our stiffest sword and the Spanish sword was the most pliable. The experimentally resolved operational deflection shapes were used to isolate the rigid body modes so that they are not reported in Figure 6 or Table 1.

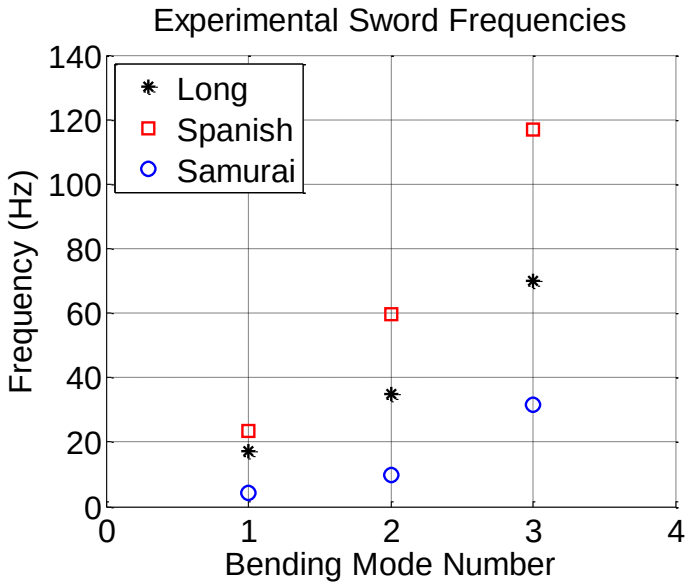

Figure 7. From averaging all the experimental trials of each sword we derived the first three, non-rigid body mode, resonant frequencies.

Since the sweet spot analysis requires us to look at only the first two bending modes we isolated the first two frequencies seen in Figure 7 for each sword. The corresponding frequency value and data location was used to extract our experimental operational deflection shapes. We report the shapes for each sword using the generalized Equation 1.

$$S_m = \frac{\frac{T_m^A * \cos(P_m^A)}{T_{max}^A} + \frac{T_m^B * -\cos(P_m^B)}{T_{max}^B}}{2} \qquad for\ m = 0,1,2,\dots,20 \tag{1}$$

Where T is the magnitude of the transfer function, P is the phase values, A/B refer to the specific measurement point, m is the hammer index, and S is the final shape value normalized by the maximum velocity of each data set and average over both measuring points for each indexed hammer hit. The values were normalized and based on the velocities because we are not as interested in magnitude as in node locations and where there is zero velocity there is zero displacement. Figure 8 and 9 shows the first and second bending mode shapes for the long sword and Spanish sword respectively. The black line represents the bottom of the guard location and the red lines are the zero axes for reference because the locations where the blue shape lines intersect the zero line is the placement of the vibrational node. A third order polynomial curve fit in a least squares sense was used to derive the actual shapes shown below. At this point we choose to disregard the Samurai sword for nodal analysis because the curvature of the sword allowed for bending modes accompanied by a heaving/torsional bending that can be seen in Figure 10. Therefore we could not experimentally resolve a pure first and second bending mode for the sword to complete a sweet spot analysis. For this reason we will leave it out of any further discussion.

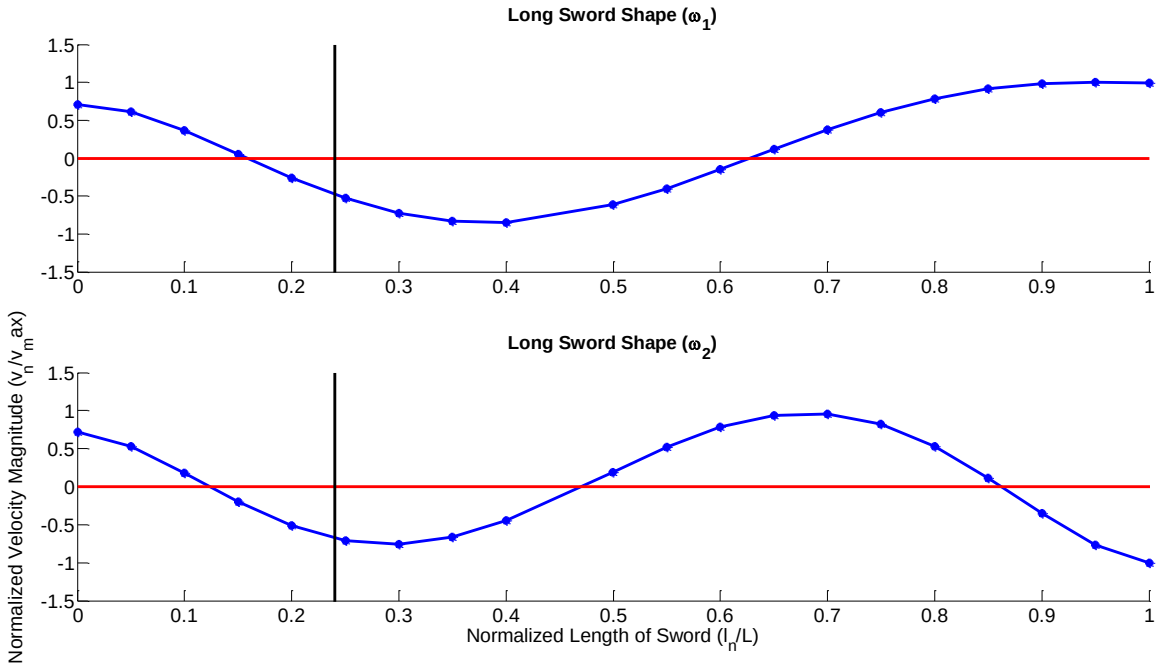

Figure 8. The mode shapes for the 1st and 2nd bending modes of the long sword. The black line represents the guard location and the red line is the zero axis.

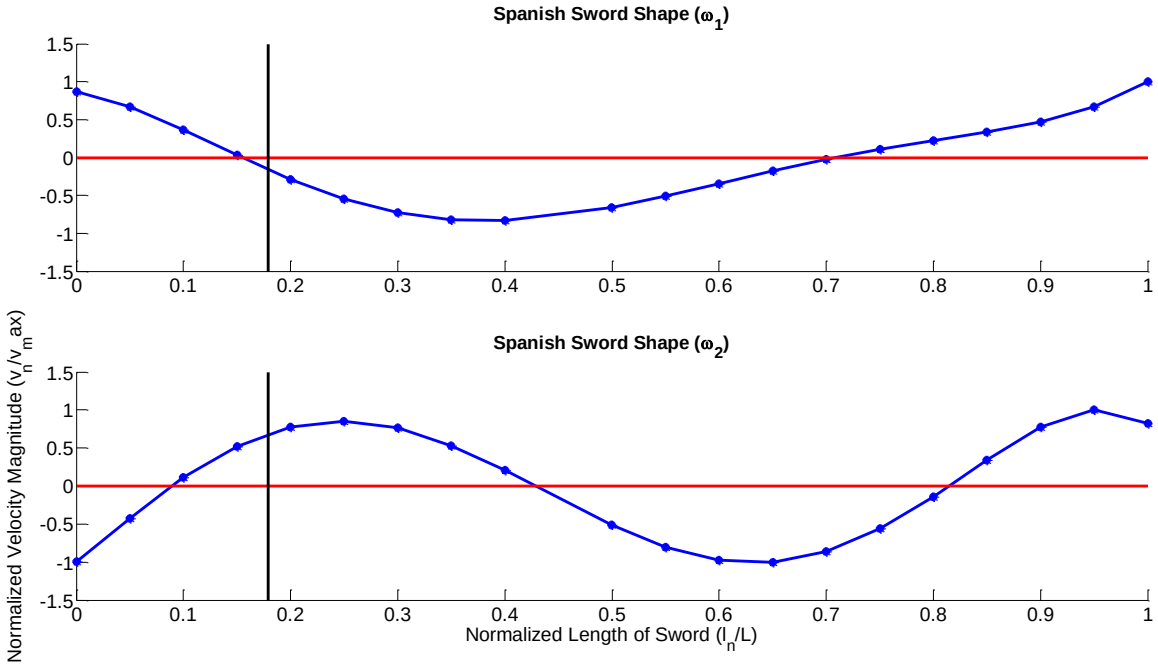

Figure 9. The mode shapes for the 1st and 2nd bending modes of the Spanish sword. The black line represents the guard location and the red line is the zero axis.

Finite Element Analysis

As a result of our simulations, the natural frequencies of first three bending modes are shown for the long and Spanish swords in Table 1. Compared to the experimentally determined natural frequencies, the simulation frequencies are significantly different. Several more FEA iterations were performed in attempt to correct the errors by changing unknown material properties to match the sword weights and increasing mesh size to resolve sensitivity to meshing, but this proved to be unsuccessful at trying to accurately predict the natural frequencies. In addition to unknown material properties causing error, the geometry of the tang was unknown for all of the swords, which also has a large effect on modal frequency predictions.

Table 1. Natural frequencies of the two swords used in our sweet spot analysis from experiments and simulation couple with the associated difference as a percentage of the experimental frequency.

Mode	Long Sword			Spanish Sword		
	EXP (Hz)	FEA (Hz)	DIF (%)	EXP (Hz)	FEA (Hz)	DIF (%)
1	17.31	12.34	28.73	23.61	34.56	46.39
2	35.06	42.51	21.25	59.60	104.47	75.28
3	69.84	91.28	30.69	117.03	262.00	123.88

For thoroughness the first two mode shapes for the three swords are shown in Figure 10. The Samurai sword is shown here to highlight the torsional or heaving effect cause by the sword curvature. It will still be disregarded for our final analysis. Node locations can be seen in dark blue for each image. We make a note that for the first and second mode of each sword, nodes appear in the hilt, showing the damping effect on vibrational magnitude created by the wooden handle, lessening the force transmitted to the sword wielder's hand(s).

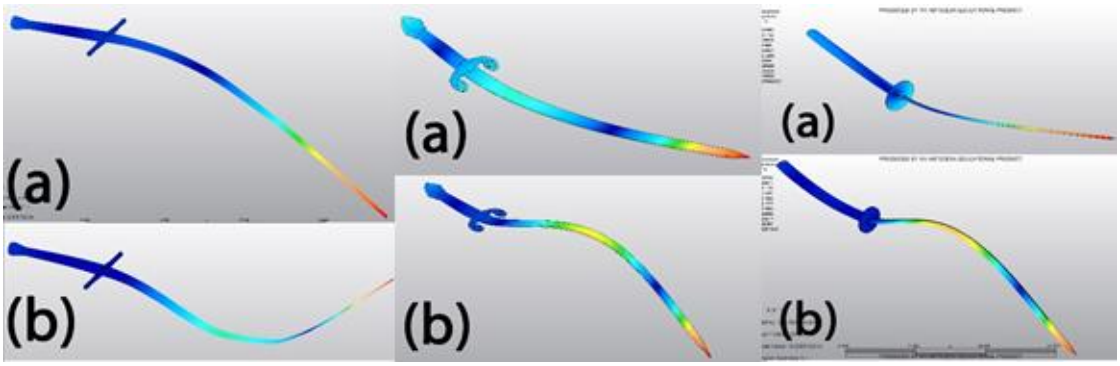

Figure 10. Composite image displaying the first 2 bending mode shapes of the three swords.

DISCUSSION AND CONCLUSIONS

FEA and Experimental Comparisons

Table 1 has already shown the numerical difference in the resolved natural frequencies. We have concluded that this could be due to multiple sources of model errors. The material properties of each sword was not intimately known and were approximated in the model. The depth of the tang in the hilt was not known for any of the swords as well and was given a standard value of 100% penetration. Experimentally the swords were not perfectly assembled and had extra range of motion at each of the connecting joints of the hilt to blade and guard to hilt. Our approximation of a reciprocal system may have been an invalid assumption as well. Figure 11 shows the percentage of difference between the experimentally and FEA resolved frequencies.

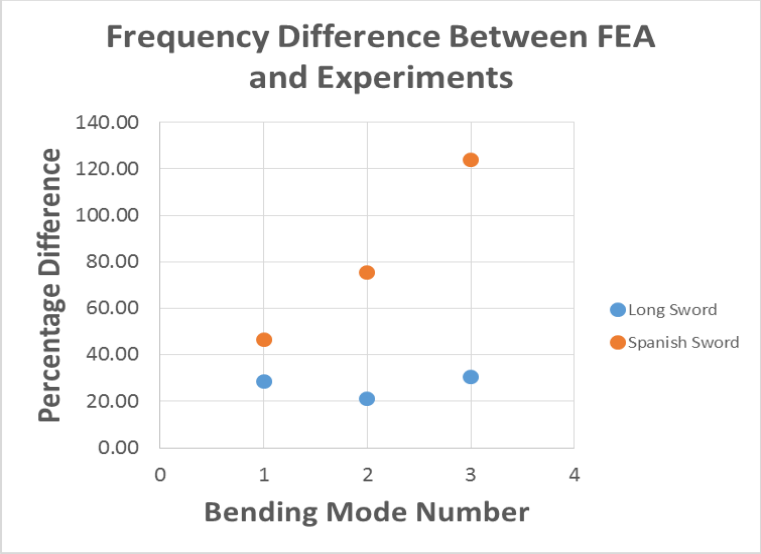

Figure 11. The difference between FEA and experimental frequencies is plotted here as a percentage of the experimental frequencies because we are more confident in their correctness.

From Figure 11 we see an offset of approximately 20 Hz between the experiments and FEA values. Since this value is not increasing in difference as a function of mode number this may just be an error in material properties and stiffness. The Spanish sword shows a two to one linear increase in the error between frequencies and the mode number increases plus a bulk offset. The reasoning for this is currently unknown to us and would require further simulation iterations. Because the frequencies were so different the deflection shapes of the FEA simulations were not used to make quantitative conclusions on

each sword design. Figure 12 and 13 shows the shapes for the model (top) and experiments (bottom) to illustrate the difference in nodal points. For these figure the nodal or zero points are highlighted by the dark blue contours.

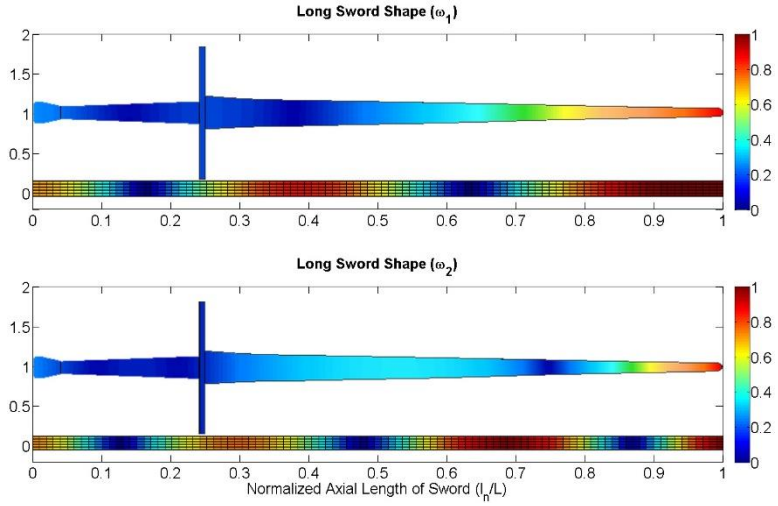

Figure 12. Contour plots of the velocity magnitudes as seen in simulations and experiments for the long sword. The linear configurations represent the experiments and the sword outline is the simulation.

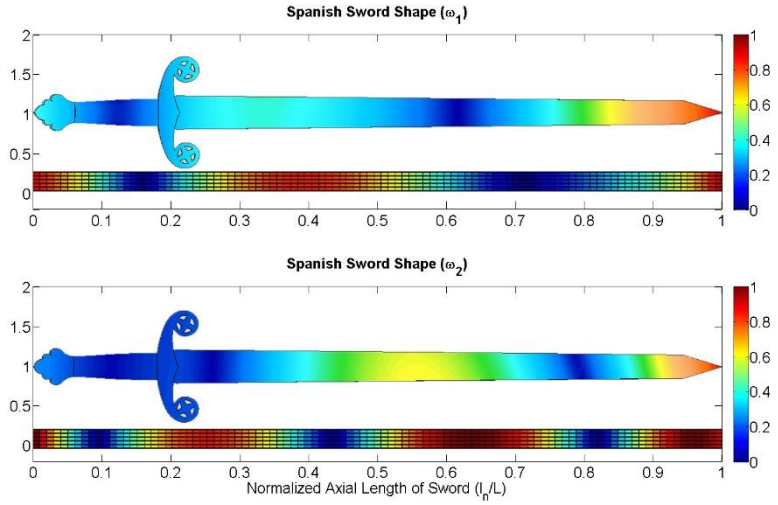

Figure 13. Contour plots of the velocity magnitudes as seen in simulations and experiments for the Spanish sword. The linear configurations represent the experiments and the sword outline is the simulation.

The final conclusion of this work in terms of the modeling is that a simpler model should have been used in the initial stages of this project. Simplifying the sword geometry to a tapered beam with three segments of equivalent mass and stiffness would have reduced geometrical complication and allowed us to use a more robust simulation program (i.e. ANSYS). Starting simple would have allowed quicker trouble shooting and iteration of mesh sizing and material properties.

Sweet Spot and Sword Design

Moving away for the FEA model we will look at the experimental deflection shapes provided in Figures 8 and 9 to draw conclusions about sword design and our sweet spot analysis. Each node location seen in the above mentioned figures has been transferred to Table 2. For each sword the first bending

mode has one hilt node and one blade node. The second bending mode has one hilt node and two blade nodes.

Table 2. Location information by the percentage of total sword length of the fundamental vibrational nodes. This is presented for the first and second modes of the long and Spanish sword.

Sword	Bending Mode	Hilt Node (%)	1st Blade Node (%)	2nd Blade Node (%)
Long	1st	15.87	62.80	
	2nd	12.28	47.17	86.27
	Difference	**3.59**	**15.63**	**23.47**
Spanish	1st	15.45	70.78	
	2nd	8.90	42.85	81.45
	Difference	**6.55**	**27.93**	**10.67**

For both swords and both bending modes the hilt node are below the guard. This can also be seen in Figures 8 and 9. The difference of the first and second mode's node is shown in the first difference column of Table 2 in percentage of sword length. Each sword creates a sweet zone which is smaller than the width of our own hands so a single hand could be within both nodes simultaneously. This is indicative of a good design in both because if either mode is excited than the user in holding on to a point of the sword where there is minimal vibration for both modes. The Spanish sword's sweet zone is closer to the guard, ideally the hand should be close or flush again the guard for zombie stabbing leverage, and this makes this a better design than the long sword.

For the hilt the distance between the nodes is less important as long as they reside in the width of one hand. The difference between the blade nodes is more important and define the region in which the user desires to hit his or her target. There is only one blade node present in the first mode but this is subtracted from both the blade nodes of the second mode to see which is closer to the node of the first mode. The closer distance is better in this sense because as the sweet zone nodes close in on each other the more likely a single strike will cancel or excite a lower energy state of the first two bending modes.

The long sword's first mode blade node is closer to the lower, guard side, blade node of the second mode. This shifts the ideal sweet zone lower down the blade and reduces the moment arm at impact yield less force transmitting to the target. The Spanish sword's first mode blade node is closer to the upper, tip side, blade node of the second mode. In the same train of thought as before this shift the ideal sweet zone towards the tip of the sword. The difference between ideal nodes is also less for the Spanish sword which marks this design, of the two considered, as the better designed sword considering both the hilt and blade and not considering reach, fighting style, and other variable which come into play as a real life fruit ninja or zombie slayer.

REFERENCES

[1] Turner, George L. "Dynamics of Hand-Held Impact Weapons." Association of Renaissance Martial Arts. (2002): V5.0.

[2] Cross, Rod. "The sweet spot of a baseball bat." American Journal of Physics 66 (1998): 772.